Eur. Phys. J. D **31**, 195–203 (2004)
DOI: 10.1140/epjd/e2004-00159-2

THE EUROPEAN PHYSICAL JOURNAL D

Prospects for the formation of ultracold ground state polar molecules from mixed alkali atom pairs

S. Azizi, M. Aymar, and O. Dulieu[a]

Laboratoire Aimé Cotton, CNRS, Bâtiment 505, Campus d'Orsay, 91405 Orsay Cedex, France

Received 2nd July 2004
Published online 23 November 2004 –

Abstract. Photoassociation rates of mixed cold alkali atom pairs and formation rates of cold heteronuclear alkali dimers in their ground state are computed within an approach where the wave functions are calculated exactly, and the laser field is treated as a perturbation. These rates are predicted to have the same magnitude for all heteronuclear species involving either Rb or Cs atoms. Moreover, these rates are found slightly smaller than, or similar to, the same rates for Cs_2 molecules, which is encouraging for future experiments. We studied the specific case of the photoassociation into excited molecular states coupled with spin-orbit interaction, emphasizing the role of the so-called resonant coupling in the formation of stable ultracold molecules with low vibrational levels. The comparison with recent experimental results on RbCs photoassociation and cold molecule formation show their reasonable agreement with our calculations.

PACS. 32.80.Pj Optical cooling of atoms; trapping – 33.20.Tp Vibrational analysis – 33.70.Ca Oscillator and band strengths, lifetimes, transition moments, and Franck-Condon factors

1 Introduction

Controlling the external and internal degrees of freedom of atomic and molecular systems is an ongoing quest of physicists for many years. Laser-cooling of ions [1] and atoms [2] represent spectacular achievements, as the external motion of the systems can be lowered down to temperatures well below 1 mK. Observation of Bose-Einstein condensation in atoms [3], and of quantum degeneracy of fermions [4], have provided the coldest gaseous samples ever observed.

However, these advances in laser cooling are not easily extended to molecules [5], due to their more complex level structure, which prevents to find a closed level scheme for population cycling. A solution has been provided via the photoassociation (PA) of ultracold atoms [6]: a pair of atoms first resonantly absorbs a photon to create an electronically excited molecule, which may then stabilizes into a long-lived electronic state by spontaneous emission [7]. The PA process is favoured due to the long-range dipole-dipole interaction between identical atoms, one being in the ground ^{2}S state, the other in the first excited state ^{2}P, varying as R^{-3} with the interatomic distance R: the absorption probability is enhanced at large distances, where the radial wave function of the colliding ultracold atoms has a large amplitude. Most achievements concern homonuclear alkali dimers observed in cold atom traps, i.e. Cs_2 [7,8], Rb_2 [9], K_2 [10], Na_2 [11]. A major advance just occurred with quantum degenerate gases, where molecules in the last bound state of the ground state potentials have been detected [12–14].

It is then highly desirable to look for news ways to forms ultracold ($T < 1$ mK) molecules of various species. The formation of ultracold dipolar molecules is particularly appealing, due to their prospected applications to quantum computation [15], or to fundamental tests like the measurement of the electron dipole moment [16,17]. The dipole-dipole long-range force is also expected to dominate the dynamics of quantum degenerate dipolar gases [18,19], with a possible control of the different quantum phases [20,21].

Promising non-optical techniques have already lead to the creation of cold molecular samples in the milliKelvin range, composed of CO and ND_3 with a Stark decelerator [22,23], and of CaH with the buffer gas cooling approach [24]. Other approaches include phase space filtering [25], supersonic expansion of a gas out of a rotating nozzle [26], or formation of dimers on helium nanodroplets [27].

An obvious possibility using one-color photoassociation (1CPA) of laser-cooled atoms, while hardly observable until recently, concerns dimers formed with different alkali atoms. In contrast with the homonuclear case, a short-range van der Waals term in R^{-6} dominates the interaction between two different alkali atoms being both in their ground state or in a different state: in order to be efficient, the PA reaction requires the atoms to approach each other at sufficiently close distances, in a region where

[a] e-mail: olivier.dulieu@lac.u-psud.fr

the initial wave function has generally a small amplitude. This experimental challenge has been successfully solved for the first time [28] with RbCs molecules. Other groups are also aiming at getting similar results with other systems like LiCs, NaLi, ... We can also quote the observation of 1CPA of the quasi-heteronuclear alkali system ^{6}Li^{7}Li [29]. Two groups have recently reported the detection of $NaCs^+$ [30,31] and KRb^+ [32] in two-species magneto-optical traps, as an evidence of the formation of the corresponding neutral cold molecules. Finally, the production of stable ultracold RbCs molecules created after 1CPA has been unambiguously reported by Kerman et al. [33], and by Wang et al. [34] for KRb molecules.

The purpose of this paper is to provide estimates for the 1CPA and cold molecule formation rates in cold heteronuclear alkali pairs, as a guidance for ongoing experiments. A first attempt to establish a hierarchy for the 1CPA efficiency for PA at small detunings of mixed alkali pairs has been proposed [35], based on a semiclassical modelling of the wave functions. Here we start instead from realistic potential curves available from the literature, to compute the wave functions of the relative radial motion of the atom pair and the reaction rates, following previous work in our group [36,37]. These rates are scaled to the cesium experimental rates, which have been carefully measured in our group [38]. We also discuss the expected vibrational distribution of the formed ultracold molecules, which could be interpreted as a probe of the actual dynamical couplings within the created molecules.

2 Model for rate calculations

We briefly recall here the main steps for the calculation of 1CPA rates and ultracold molecule formation rates, following the perturbative approach previously developed in our group [36,37], essentially equivalent to those described elsewhere [39,40]. The 1CPA rate of a pair of cold ground state atoms M,M', into a molecule MM'* excited in an electronic state Ω, expressed in s^{-1} per atom, is calculated according to:

$$\mathcal{R}_{PA}(\Delta_v) = \left(\frac{3\lambda_{th}^2}{2\pi}\right)^{\frac{3}{2}} \frac{h}{2} n_{MM'} \mathcal{A}_\Omega \left|\langle\phi(v_\Omega)|\Gamma|\chi(k_BT)\rangle\right|^2, \quad (1)$$

where Δ_v is the binding energy (or the detuning of the PA laser with intensity I) of the populated vibrational level v_Ω relative to the dissociation limit of the electronic state Ω. The atomic cloud composed of M and M' species is assumed in equilibrium at a temperature T, with a pair density $n_{MM'}$ and is characterized by the thermal de Broglie wavelength $\lambda_{th} = h\sqrt{1/(3\mu k_B T)}$ (μ is the reduced mass of the M,M' pair). The rate is determined by the Franck-Condon factor involving the initial radial continuum wave function $\chi(k_BT;R)$ and the vibrational wave function $\phi(v_\Omega;R)$ of the PA level (the brackets hold for the integral over the interatomic distance R). The molecular Rabi frequency $2\Gamma(R) = E_{PA}D(R)/\hbar$ is proportional to the molecular (R-dependent) transition dipole moment $D(R)$ and to the amplitude E_{PA} of the PA laser. The $\mathcal{A}_\Omega$ factor includes all angular factors relevant to the chosen approximations and experimental arrangement (choice for the laser polarization). We assume that the (M,M') pair collides in the s-wave, and that its rotational angular momentum is decoupled from its internal angular momenta. At this point, we also neglect the hyperfine structure of the atoms.

The cold molecule (CM) formation rate:

$$\mathcal{R}_{CM}(\Delta_v) = \mathcal{R}_{PA}(\Delta_v) B(v_\Omega) \quad (2)$$

is proportional to the PA rate, and to the branching ratio $B(v_\Omega)$ for spontaneous emission of the v_Ω level into the vibrational levels v'' of the lowest allowed electronic state of the molecule:

$$\begin{aligned} B(v_\Omega) &= \frac{1}{A(v_\Omega)} \sum_{v''} A_{v_\Omega v''} \\ &= \frac{1}{A(v_\Omega)} \sum_{v''} \frac{4e^2\omega_{v_\Omega v''}^3}{\hbar c^3} \left|\langle\phi(v_\Omega)|D|\phi(v'')\rangle\right|^2 \end{aligned} \quad (3)$$

where $\omega_{v_\Omega v''}$ is the frequency of the emitted photon, and $A(v_\Omega)$ the total spontaneous emission probability. Assuming that $D(R)$ is slowly varying with R, and that the energy range of the populated v'' levels is small compared to the magnitude of $\hbar\omega_{v_\Omega v''}$, the branching ratio can be approximated by:

$$B(v_\Omega) = \sum_{v''} \left|\langle\phi(v_\Omega)|\phi(v'')\rangle\right|^2. \quad (4)$$

The main interest for studying ultracold molecules formed from different alkali atoms appears clearly from equations (2–4): in contrast with an homonuclear pair, the spontaneous emission from the PA state is favoured at short distances since both the ground state (or the accompanying lowest triplet state) and the excited potential curves vary as R^{-6}, giving a good opportunity to populate vibrational levels of the ground state. Another general motivation is to create stable ultracold molecules in vibrational levels as bound as possible, and ultimately in the lowest vibrational level $v = 0$. Dion et al. [37] have shown that the so-called "resonant coupling", resulting from the non-Born-Oppenheimer interaction between two electronic states, is a good candidate for such a goal. The coupling between two potential curves may induce an enhancement at quite short distances of the probability density in the PA level, giving access to low vibrational levels after the spontaneous decay step. Dion et al. applied this model to the formation of ultracold cesium dimers, which involves the strong spin-orbit interaction between the two excited states $A^1\Sigma_u^+$ and $b^3\Pi_u$ correlated to the Cs(6s)+Cs(6p) dissociation limit. In Hund's case c coupling scheme, these states are labeled as belonging to the 0_u^+ symmetry and dissociate into Cs(6s)+Cs(6$p_{1/2,3/2}$). Several other works have also shown that the spin-orbit interaction in the heavy alkali atoms Rb and Cs is responsible for the strong perturbation of the dimer vibrational spectrum in their excited states, which requires to treat

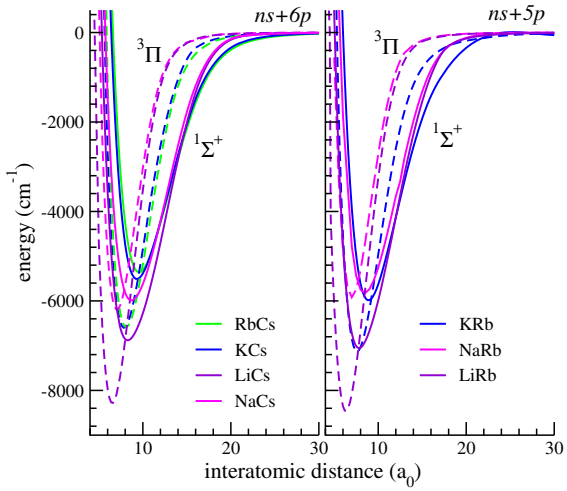

Fig. 1. The $A^1\Sigma^+$ (full lines) and $b^3\Pi^+$ (dashed lines) curves for mixed-alkali dimers containing (a) Cs and (b) Rb. References for these data are given in the text. A color version of the figure is available in electronic form at `www.eurphysj.org`.

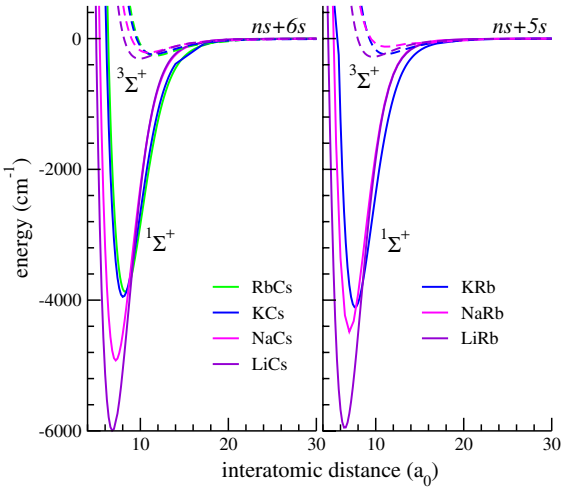

Fig. 2. The $X^1\Sigma^+$ (full lines) and $a^3\Sigma^+$ (dashed lines) curves for mixed-alkali dimers containing (a) Cs and (b) Rb. References for these data are given in the text. A color version of the figure is available in electronic form at `www.eurphysj.org`.

simultaneously both A and b states and their coupling for the vibrational assignment [41,42]. So we expect that the resonant coupling induced by the spin-orbit interaction between the similar states of the mixed compounds MRb or MCs (with M = Li, Na, K, including also RbCs), denoted by $A^1\Sigma^+$ and $b^3\Pi$ will also be efficient. We will focus on the A and b states of these heavy species in the following. As for the homonuclear case, the Hund's case c coupling scheme assigns the 0^+ symmetry to these states.

Wang and Stwalley [35] extensively recalled in their paper the basic properties of the electronic potential curves of the heteronuclear alkali-metal diatomic molecules, especially their large-distance part. Briefly, such molecules have two lowest excited $^2S + {}^2P$ asymptotes which split into four fine-structure asymptotes $^2S_{1/2} + {}^2P_j$, with $j = 1/2, 3/2$. Numerical data for these potential curves are available in the literature, and we use here results from the following references: reference [43] (LiCs, NaCs, KCs), reference [44] (RbCs), reference [45] (LiRb, NaRb), and reference [46] (KRb).

The potential curves correlated to the lowest $^2S + {}^2P$ asymptote, which corresponds to M(ns)+Cs($6p$) (with M = Li, Na, K, Rb), and to M(ns)+Rb($5p$) (with M = Li, Na, K), behave similarly to those of the homonuclear systems. For instance, Figure 1 displays the $A^1\Sigma^+$ and $b^3\Pi$ curves for Cs and Rb compounds, which are expected to undergo spin-orbit coupling due to their short-range crossing. At large distances where PA takes place, these states have a dominant 0^+ Hund's case c character. Due to their mixed singlet-triplet character, they are both accessible from the ground state $X^1\Sigma^+$ and the lowest triplet state $a^3\Sigma^+$ dissociating into the $^2S+{}^2S$ ground state asymptote (Fig. 2).

Just like homonuclear dimers, the asymptotic behavior of the $^2S+{}^2P$ excited potential curves is different from one mixed pair to another. The coefficient C_6 of the leading term in R^{-6} of their long-range expansion [47] has the largest value for KRb, RbCs, and KCs, which lead Wang and Stwalley [35] to suggest that for small PA detunings the photoassociation process will be more favorable for these latter species by at least one order of magnitude than for all the others due to their enhanced attractive character at large R. In the next section, we investigate this statement for large PA detunings using exact wave functions in the rate expression, instead of the semiclassical approach of reference [35].

3 Results

3.1 Definition of rescaled rates

In equations (1, 2), typical experimental conditions must be defined to compute the rates. We assume here that PA experiments could be performed under temperature and atomic density conditions similar to those achieved for the Cs_2 experiment of the Orsay group [7]. As $\mathcal{R}_{PA}$ and $\mathcal{R}_{CM}$ have been carefully measured for Cs_2 [38], we define a reduced PA rate for Cs_2 according to $\bar{\mathcal{R}}_{PA}(Cs_2) = |\langle\phi_{CsCs}(v_\Omega)|\Gamma|\chi_{CsCs}(k_BT)\rangle|^2$, where all fundamental constants and experimental parameters have been left out. The computed PA rates for heteronuclear dimers can now be rescaled to the Cs_2 rates, by defining:

$$\bar{\mathcal{R}}_{PA}(MM') = \left(\frac{\mu_{CsCs}}{\mu_{MM'}}\right)^{3/2} \alpha_{at}^2 \times |\langle\phi_{MM'}(v_\Omega)|\chi_{MM'}(k_BT)\rangle|^2 . \quad (5)$$

Equation (5) depends on the Franck-Condon (FC) factor relevant for each system, and then emphasizes the role of the differences for each M,M' pair between the potential curves behavior. But comparing the FC factor for MM' to the Cs_2 one is not sufficient to obtain an estimate

for the rate, as other factors depending on the reduced mass and on the transition dipole moment are involved. Since PA occurs mainly at large R, the molecular transition dipole moment has been replaced in $\Gamma(R)$ by the atomic one for the relevant atomic transition. This is accounted by the scaling factor α_{at}, equal to 1 for LiCs, NaCs, KCs, RbCs, and to the ratio of atomic Rabi frequencies $\alpha_{at} = \Gamma_{\rm Rb}(5s \rightarrow 5p)/\Gamma_{\rm Cs}(6s \rightarrow 6p) \approx 0.9$ for LiRb, NaRb, KRb. Numerical values for the scaling factor involving reduced masses in equation (5) are listed in Annex (Tab. 1) for these pairs, considering various isotopic combinations. Finally, as we neglect the atomic hyperfine structure, we have not included in equation (5) the ratio of $\mathcal{A}_\Omega$ factors. In reference [38], this factor has been evaluated for Cs_2 photoassociation in the 0_g^- and 0_u^+ symmetries, assuming a linear polarized PA light and s-wave incoming channel. The ratio $\mathcal{A}(0_u^+(P_{1/2}))/\mathcal{A}(0_g^-(P_{3/2}))$ is found equal to 0.29, 0.77, and 0.28 according to the chosen initial combination of atomic total angular momentum $(F, F') = (3,3), (3,4), (4,4)$ respectively. One may assume that the ratio $\mathcal{A}(0^+(P_{1/2}))/\mathcal{A}(0_g^-(P_{3/2}))$ relevant for the present study will take similar values, and that the rates computed for the mixed species, displayed in the following figures, could be changed by a similar amount when they are compared to the Cs_2 $0_g^-(P_{3/2})$ rates.

The rescaled CM rate can now be written following equation (2):

$$\bar{\mathcal{R}}_{CM}(MM') = \bar{\mathcal{R}}_{PA}(MM')B(v_\Omega). \qquad (6)$$

The main task is now the numerical computation of wave functions, achieved just like in reference [37]: continuum wave functions are determined from a standard Numerov integration algorithm, for a temperature T =140 μK typical of the PA experiment in cesium [7]. Vibrational wave functions and energies are obtained from our Fourier Grid Hamiltonian code described elsewhere [42,48], which is well adapted to the solution of the coupled state problem under study. We focus on the $X^1\Sigma^+ \rightarrow 0^+(A^1\Sigma^+)$ and $a^3\Sigma^+ \rightarrow 0^+(b^3\Pi)$ transitions in our list of heavy mixed pairs, for both the PA and CM rates. These notations refer to the component of the coupled 0^+ states which is allowed for dipolar transition selection rule.

We evaluate these rates for photoassociated levels with a binding energy between 1 cm^{-1} and 30 cm^{-1}, typical of PA experiments in standard magneto-optical traps. Levels bound by less than 1 cm^{-1} are strongly affected by the hyperfine structure, and the present calculations are no more significant. At large internuclear distances, we smoothly connected the quantum chemistry potential curves displayed in Figures 1 and 2 to asymptotic expansions $\sum_n C_n/R^n$, using the accurate asymptotic C_n coefficients of reference [47]. The scattering length of the $^2S+^2S$ resulting potentials is arbitrary, and not relevant for our purpose, as long as they are not too large. The 2×2 Hamiltonian describing the 0^+ states (see for instance Ref. [37]) involves either the Rb or Cs atomic spin-orbit interaction, or a model function $\zeta(R)$ for the R-dependent molecular spin-orbit coupling. Indeed, as no molecular data is available for this latter quantity, we follow the same approach

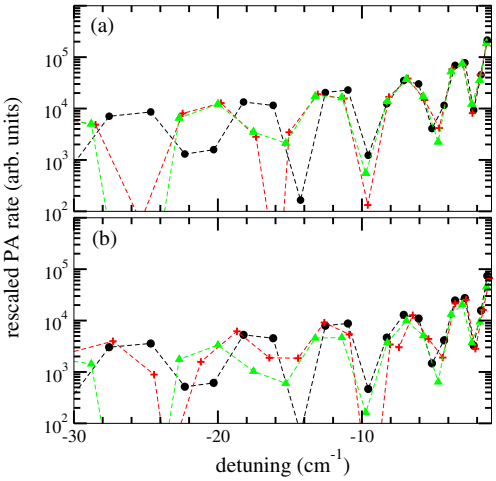

Fig. 3. Rescaled rates (a) for photossoasociation and (b) cold molecule formation for the $X^1\Sigma^+ \rightarrow 0^+(A^1\Sigma^+)$ transition in RbCs, under the three assumptions (i) single state calculation (in green with triangles), (ii) coupled state calculation with atomic spin-orbit coupling (in red with plus signs), (iii) coupled state calculation with variable spin-orbit coupling (in black with circles). These different cases are defined in the text. The dashed lines are displayed to guide the eye. A color version of the figure is available in electronic form at `www.eurphysj.org`.

than in reference [49]: we use for the Cs compounds the $\zeta_{\rm Cs}(R)$ function from the quantum chemistry results of Spies [50] on Cs_2 0_u^+ states. For Rb compounds we rescale the coupling to $\zeta_{\rm Rb}(R) = \zeta_{\rm Cs}(R)\Delta_{so}({\rm Rb})/\Delta_{so}({\rm Cs})$, by the ratio of atomic fine structure splittings, as no calculation is available.

3.2 Photoassociation rates

As a typical example, we first check some of our hypothesis on RbCs rates (Fig. 3). Since the molecular spin-orbit interactions are almost unknown, we calculated the PA rate assuming that (i) the single $0^+(5^2S + 6^2P_{1/2})$ potential is effective for PA, (ii) both 0^+ potentials are effective, coupled through atomic spin-orbit interaction, (iii) or by the R-dependent spin-orbit interaction defined above. We see that the rates have almost the same magnitude for all cases, which actually reflects the conclusion of reference [37] for the resonant coupling between 0_u^+ states in Cs_2. The approximation used here for the unknown coupling term is then not crucial for the remaining of the discussion.

The reduced PA rates for Cs and Rb compounds calculated for the transition $X^1\Sigma^+ \rightarrow 0^+(A^1\Sigma^+)$ using the $\zeta_{\rm Cs}(R)$ and $\zeta_{\rm Rb}(R)$ coupling functions are displayed in Figure 4. It is striking to see that rescaled PA rates for all species differ by at most a factor 4. This contrasts with reference [35], where the authors obtained for small PA detunings overlap integrals larger by orders of magnitude for heavy species, compared to the light ones. But despite the large value of the leading asymptotic coefficient C_6 in the PA state, compared to the C_6 coefficient in the ground

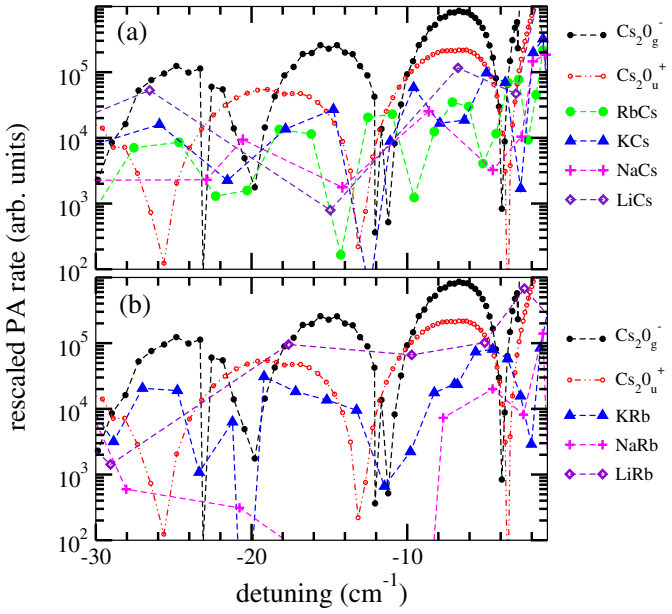

Fig. 4. Rescaled photoassociation (PA) rates for(a) Cs compounds and (b) Rb compounds, for the $X^1\Sigma^+ \rightarrow 0^+(A^1\Sigma^+)$ transition, as a function of the detuning of the PA laser below the relevant $^2S + ^2P_{1/2}$ asymptote. The temperature is fixed to 140 μK for the initial colliding pair of atoms. They are compared to reduced PA rates for the $a^3\Sigma_u^+ \rightarrow 0_g^-(6^2S + 6^2P_{3/2})$ and $X^1\Sigma_g^+ \rightarrow 0_u^+(6^2S + 6^2P_{1/2})$ transitions in Cs_2. A color version of the figure is available in electronic form at `www.eurphysj.org`.

state, the density of levels in the present detuning range is not large enough for the reflection approximation to be accurate [39], i.e. the quantum calculation of the full wave functions is required, instead of their values at the outer turning point of the PA level. However, as in reference [35], our computed overlap integral for the heavier species KRb, KCs, RbCs are still predicted to be larger than the lighter species LiRb, LiCs, NaRb, and NaCs. Finally the reduced mass scaling factor present in the rescaled rates balances this hierarchy, and tends to slightly favour the lighter species. This results is in qualitative agreement with the weak $\mu^{-1/2}$ dependence found in the perturbative model of reference [36]. Although not surprising, the comparison with the PA rate for the $a^3\Sigma_u^+ \rightarrow 0_g^-(6^2S + 6^2P_{3/2})$ transition in Cs_2 is found about 10 to 30 times smaller for the heteronuclear species. This is due to the shorter range of their excited molecular potentials (varying as R^{-6} at large distances), compared to the homonuclear case (in R^{-3}). The same qualitative conclusion holds also for the PA rates of $a^3\Sigma^+ \rightarrow 0^+(b^3\Pi)$ transition (not displayed here), which are predicted to be 5 to 20 times smaller than the Cs_2 ones. It should be noted that PA signal from the $0_g^-(6^2S + 6^2P_{1/2})$ state of Cs_2, which behaves also as R^{-6} at large distances, has been observed in reference [51], with a magnitude well below the one for the $0_g^-(6^2S + 6^2P_{3/2})$ state.

Together with the preceding example, the rate for the $X^1\Sigma_g^+ \rightarrow 0_u^+(6^2S + 6^2P_{1/2})$ transition in Cs_2, which represents the resonant coupled state case in Cs_2 equivalent to the situation studied with mixed species here, provides an indication on the typical range for PA rates in Cs_2, which may vary by a factor of about 5 depending on the considered PA state: experimentally, an interval of 1 to 5 s^{-1} per atom has been measured [38].

Finally it is interesting to try to express these results in terms of measurable rates, in order to compare them to experimental values. In reference [38], the PA rate for the $v = 77$ level of the $0_g^-(6^2S + 6^2P_{3/2})$ external well in Cs_2, located at a detuning of about 7 cm^{-1}, was measured around 1.25×10^8 s^{-1} (with a factor of 2 uncertainty linked to the determination of the absolute number of atoms $N_{Cs} = 5 \times 10^7$), for a PA laser intensity $I = 55$ Wcm^{-2}, and an atomic cloud with a temperature of 140 μK; in the same paper, the same perturbative model than the one used here yields a value of about 2.5×10^8 s^{-1}, in good agreement with the experimental value. In the recent PA experiment on RbCs of reference [28], the authors reported a rate of about 1.5×10^8 s^{-1}, measured on PA lines saturating for a laser intensity of 100 Wcm^{-2}, and using larger sample of cold atoms $N_{Rb} = 4 \times 10^8$ and $N_{Cs} = 3 \times 10^8$ with temperature $T_{Rb} = 55$ μK and $T_{Cs} = 140$ μK respectively. Our calculation in Figure 4 indicates that the PA rate for 0^+ levels of RbCs is about 30 times smaller than for the $0_g^-(6^2S + 6^2P_{3/2})$ levels in Cs_2, assuming similar experimental conditions. This predicted difference in the rate magnitude agrees quite well with the experiments, if we assume [36] that the rate is proportional to the PA laser intensity (which is larger by a factor of 2 in the RbCs experiment), to the atom number (which is larger by a factor of 10 in the RbCs experiment), and to the inverse of the temperature (which brings a factor between 1 and 2, difficult to estimate as the two species are not at the same temperature in the RbCs experiment).

3.3 Cold molecule formation rates

The rescaled cold molecule formation rates depend on the branching ratio $B(v_{0^+})$ towards the lowest electronic states, displayed in Figure 5, which are slowly varying functions of the detuning of the PA level: indeed, the wave function of the PA level has noticeable overlaps with several vibrational wave functions of the ground state, which all sum up into $B(v_{0^+})$ where the details of the individual wave functions are smoothed. For the lighter species involving Li and Na, irregularities are still visible, as the density of levels in the ground state is weaker than for the heavier species. As inferred in the first section, the branching ratio for the mixed species is larger than for Cs_2, which reflects that the similar R^{-6} asymptotic behavior of the lowest potential curve and of the excited potential curves favours the spontaneous emission, compared to the Cs_2 case.

The rescaled cold molecule (CM) formation rates are reproduced in Figure 6. As already discussed in reference [38], the slow increase of the branching ratio with increasing detunings compensates the decreasing of the rescaled PA rate, leading to a CM rate which has an

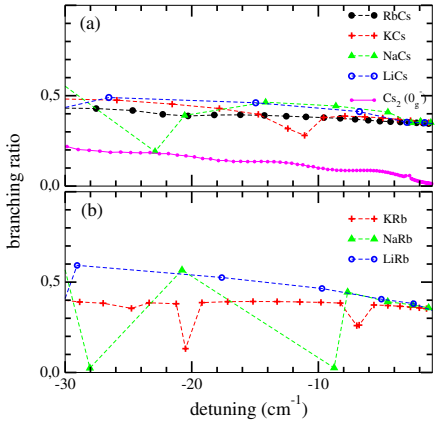

Fig. 5. Branching ratio of the $X^1\Sigma^+ \leftarrow 0^+(A^1\Sigma^+)$ transition for (a) Cs and (b) Rb compounds. In (a), the branching ratio for the $0_g^-(6^2S + 6^2P_{3/2}) \rightarrow a^3\Sigma_u^+$ transition in Cs_2 is also indicated. A color version of the figure is available in electronic form at `www.eurphysj.org`.

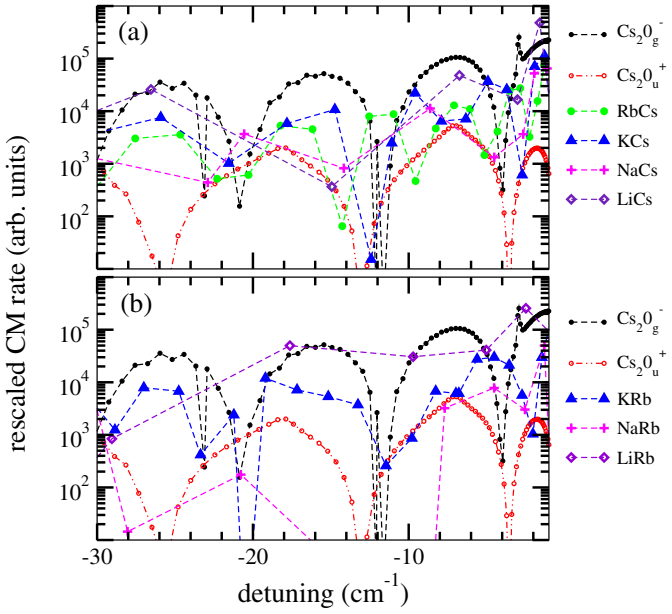

Fig. 6. Rescaled cold molecule formation (CM) rates for(a) Cs compounds and (b) Rb compounds, for the $X^1\Sigma^+ \rightarrow 0^+(A^1\Sigma^+)$ transition, as a function of the detuning of the PA laser below the relevant $^2S + ^2P_{1/2}$ asymptote. The temperature is fixed to 140 μK for the initial colliding pair of atoms. They are compared to reduced CM rates for the $a^3\Sigma_u^+ \rightarrow 0_g^-(6^2S + 6^2P_{3/2})$ and $X^1\Sigma_g^+ \rightarrow 0_u^+(6^2S + 6^2P_{1/2})$ transitions in Cs_2. A color version of the figure is available in electronic form at `www.eurphysj.org`.

almost constant average magnitude over the displayed range. The spontaneous emission probability towards bound levels of the ground state is favoured for the mixed dimers compared to the homonuclear ones, so that the CM rate is predicted to have a magnitude at most 10 times smaller than the rate observed for Cs_2, which is encouraging for future experiments. Again, our calculations lead to the same conclusion for the triplet transition.

As in the previous section, we can relate the calculated rates to available experimental values: the formation rate of Cs_2 ultracold molecules after PA of the $0_g^-(6^2S+6^2P_{3/2})$ levels is found around 2×10^6 s^{-1} [38], while a value of 10^6 s^{-1} is reported for RbCs [33]. If we rely again on the factor of about 30 induced by the differences in the experimental conditions, the formation rate for RbCs ground state molecules is found about 15 times smaller than for Cs_2, while Figure 6 shows that the calculated rates differ by a factor around 10. The agreement is then satisfactory, and our model predicts that formation of LiRb and LiCs ultracold ground state molecules should be four times more efficient than for RbCs molecules.

The comparison with experiments in KRb [32], NaCs [30], and NaRb [31] is not discussed here, as these experiments rely on a PA step performed with the trapping lasers, at very small detunings. Moreover, no PA rate is available in the most recent KRb experiment of Wang et al. [34].

3.4 Vibrational distributions of ultracold molecules

The branching ratio $B(v_{0^+})$ is defined as the sum of the overlap integrals between the PA vibrational wave function and the wave functions of the populated levels in the ground state. It is worthwhile to look at the individual integrals, as it enlightens the vibrational distribution of the formed ground state ultracold molecules. The computed distribution in the RbCs case is given in Figure 7, considering a single channel model (case (i) above), and a coupled channel calculation with a variable coupling (case (iii) above). This clearly illustrates now the crucial role of the resonant coupling studied here: in the absence of this coupling (case (i)), only the highest vibrational levels of the ground state are populated. In contrast, a significant amount of ultracold molecules are created in deeper vibrational levels for case (iii), as the resonant coupling induces in the PA wave function a Condon point at intermediate distances, which favours the spontaneous emission towards these levels. This was the main result of reference [37], where the observation of PA lines below the $6S + 6P_{1/2}$ asymptote was interpreted as a clear evidence of the presence of the resonant coupling between levels of the two 0_u^+ states coupled with spin-orbit interaction. Kerman et al. interpreted [33] their observations in the same way, and predicted a rate of about 5×10^5 s^{-1} (corresponding to $\approx 1.5 \times 10^4$ s^{-1} for experimental conditions of reference [38] using again the factor 30 above) for the formation of ground state RbCs molecules in the level $v = 62$ bound by almost 1300 cm^{-1}. As represented in Figure 7, our calculations predict that the lowest populated level in the ground state is around $v = 55$, bound by almost 1400 cm^{-1}, with a Franck-Condon factor of 0.001, out of a total branching ratio of $\approx$0.4. Under conditions similar to those of reference [38], it would correspond to a rate of 5×10^3 s^{-1}, in reasonable agreement with reference [33]. The differences in the vibrational assignement is probably due to the choice of the 0^+ molecular potentials and of their coupling.

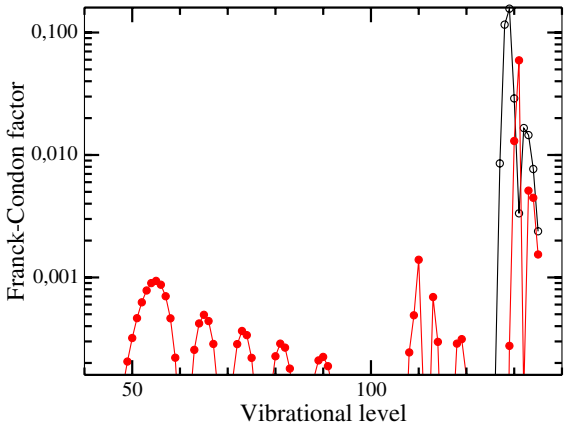

Fig. 7. Vibrational distribution of cold RbCs molecules in the $X^1\Sigma_g^+$ ground state, after spontaneous emission from the PA level of the 0^+ state located at a 7 cm^{-1} detuning. The abcissa shows the vibrational quantum number of the ground state levels. Open circles: case (i), single-state calculation; closed circles: case (iii), two-coupled-state calculation (see text).

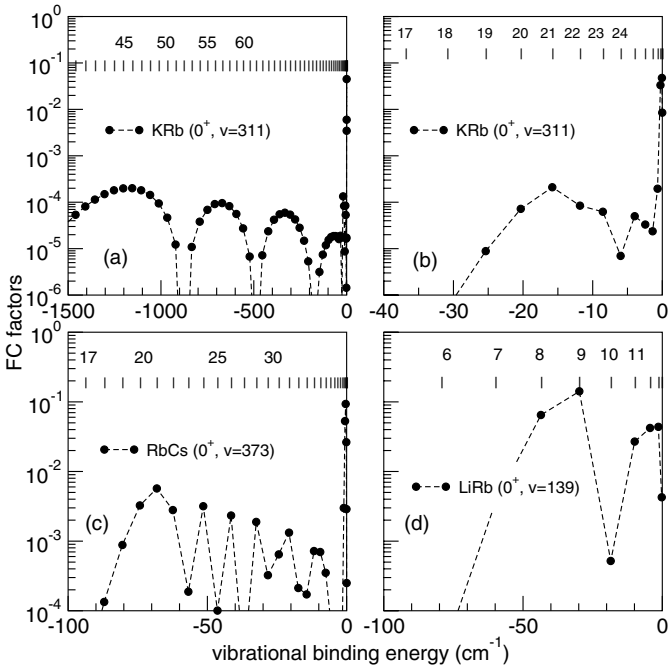

Fig. 8. Various examples of vibrational distribution of cold molecules, expressed as Franck-Condon (FC) factors computed in case (iii) defined previously, as a function of the binding energy of the vibrational levels of the singlet ground state (a), or of the lowest triplet state (b), (c), and (d). The corresponding numbering of the levels is also given in the upper part of each figure. The initial PA level of the excited molecule is indicated by its rank in the eigenvalues of the coupled 0^+ states. In each case, the chosen level corresponds to a detuning where the cold molecule formation rate is maximum: (a) and (b) ≈5 cm^{-1}, (c) ≈8 cm^{-1}, (d) ≈2.5 cm^{-1}.

The vibrational distributions depend on the final molecular state (singlet or triplet), and on their scattering length which is arbitrary here, as well as on the PA level and on the strength of its resonant coupling with neighbouring levels. We present in Figure 8 several examples which illustrates different situations. Generally, the most populated levels are still by far those which are close to the dissociation limit. Deep vibrational levels of the RbCs lowest triplet state are expected to be efficiently populated (see Fig. 8c) due to the resonant coupling in the PA level, as for the singlet case of Figure 7. In contrast, the low vibrational levels in KRb seem more difficult to reach in the present model (see Figs. 8a and 8b): this is probably due to the large C_6 asymptotic coefficient of the PA state, which will favour spontaneous emission at large distances. The LiRb molecule seems to provide a valuable case where the vibrational distribution could be concentrated on a few levels of the lowest triplet state.

4 Conclusion

In this paper, we have shown that the photoassociation of cold mixed alkali atom pairs and the subsequent formation of cold molecules is a promising experimental investigation, as our calculations predict rates for these processes which have a magnitude comparable to the rates previously measured for Cs_2 molecules. Our results are also in agreement with the most recent observations on cold RbCs molecule formation. An important statement is the necessity to compute exactly the vibrational wave functions over their whole radial extension, and not only at the vicinity of their classical outer turning point. Reliable quantitative comparisons of rate magnitude among different pairs are obtained when mass scaling factors are introduced in the calculations as a weight for the Franck-Condon factors involved in the rate expressions.

We also emphasize the role of the resonant coupling between vibrational levels of two coupled electronic excited states of the molecules, which is predicted to enhance the formation of cold molecules in deeply bound vibrational levels of the ground state. Such a mechanism, initially proposed by Dion et al. [37], is also invoked by Kerman et al. [33] as the first step for the formation of ultracold ground state molecules in the $v = 0$ vibrational level. The main challenge for experimentalists is now the detection of the ultracold molecules and their vibrational population, as the density of photoassociated levels is lower for heteronuclear species than for homonuclear pairs. The ionization of the created molecules is a powerful method [7], and is a necessity, as it has been clearly demonstrated for RbCs [33]. Further theoretical studies should rely either on precise molecular potential curves determined by other means, like for instance conventional absorption spectroscopy [52], high-resolution laser spectroscopy [53], spectroscopy of molecules trapped on helium droplets [27], or should suggest improvement of existing potential curves through the fit of experimental photoassociation data which are expected to come in a near future.

Table 1. Reduced masses and mass scaling factors involved in the rescaled PA rates (Eq. (5)).

MM'	$\mu(MM')$ (a.u.)	$(\mu(\mathrm{Cs_2})/\mu(MM'))^{3/2}$
^{6}LiCs	10490.137	39.24
^{7}LiCs	12148.112	31.48
NaCs	35727.701	6.24
^{39}KCs	54924.432	3.27
^{85}RbCs	94445.005	1.45
^{87}RbCs	95788.267	1.42
Cs_2	121136.005	1
^{6}Li^{85}Rb	10239.541	40.69
^{7}Li^{85}Rb	11813.306	32.83
Na^{85}Rb	32978.838	7.03
^{39}K^{85}Rb	48685.913	3.92
$^{85}Rb_2$	77392.426	1.95
^{6}Li^{87}Rb	10255.132	40.59
^{7}Li^{87}Rb	11834.063	32.74
Na^{87}Rb	33141.121	6.98
^{39}K^{87}Rb	49040.422	3.88
$^{87}Rb_2$	79212.941	1.89

Annex

We display in Table 1 reduced masses and the mass scaling factors $(\mu(\mathrm{Cs_2})/\mu(MM'))^{3/2}$ present in equation (5) for the mixed pair involving Rb and Cs. Values for different isotopes are given for clarity.

Stimulating discussions with Claude Dion and Andrea Simoni are gratefully acknowledged. This work is supported by the European Research and Training Network "Cold Molecules" (contract HPRN-CT-2002-00290). S.A. acknowledges the support of the Algerian Ministry for High Education.

References

1. J. Eschner, G. Morigi, F. Schmidt-Kaler, R. Blatt, J. Opt. Soc. Am. B **20**, 1003 (2003)
2. C.E. Wieman, D.E. Pritchard, D.J. Wineland, Rev. Mod. Phys. **71**, s253 (1999)
3. W. Ketterle, Rev. Mod. Phys. **74**, 1131 (2002)
4. C.A. Regal, C. Ticknor, J.L. Bohn, D.S. Jin, Phys. Rev. Lett. **90**, 053201 (2003)
5. J.T. Bahns, P.L. Gould, W.C. Stwalley, J. Chem. Phys. **104**, 9689 (1996)
6. H.R. Thorsheim, J. Weiner, P.S. Julienne, Phys. Rev. Lett. **58**, 2420 (1987)
7. A. Fioretti, D. Comparat, A. Crubellier, O. Dulieu, F. Masnou-Seeuws, P. Pillet, Phys. Rev. Lett. **80**, 4402 (1998)
8. T. Takekoshi, B.M. Patterson, R.J. Knize, Phys. Rev. A **59**, R5 (1999)
9. C. Gabbanini, A. Fioretti, A. Lucchesini, S. Gozzini, M. Mazzoni, Phys. Rev. Lett. **84**, 2814 (2000)
10. A.N. Nikolov, E.E. Eyler, X.T. Wang, J. Li, H. Wang, W.C. Stwalley, P.L. Gould, Phys. Rev. Lett. **82**, 703 (1999)
11. F.K. Fatemi, K.M. Jones, P.D. Lett, E. Tiesinga, Phys. Rev. A **66**, 053401 (2002)
12. J. Herbig, T. Kraemer, M. Mark, T. Weber, C. Chin, H.-C. Nägerl, R. Grimm, Science **301**, 1510 (2003)
13. S. Jochim, M. Bartenstein, A. Altmeyer, G. Hendl, C. Chin, J. Hecker Denschlag, R. Grimm, Phys. Rev. Lett. **91**, 240402 (2003)
14. C.A. Regal, C. Ticknor, J.L. Bohn, D.S. Jin, Nature **424**, 47 (2003)
15. D. DeMille, Phys. Rev. Lett. **88**, 067901 (2002)
16. M.G. Kozlov, D. DeMille, Phys. Rev. Lett. **89**, 133001 (2002)
17. J.J. Hudson, B.E. Sauer, M.R. Tarbutt, E.A. Hinds, Phys. Rev. Lett. **89**, 023003 (2002)
18. K. Góral, L. Santos, Phys. Rev. A **66**, 023613 (2002)
19. M.A. Baranov, M.S. Mar'enko, V.S. Rychkov, G.V. Shlyapnikov, Phys. Rev. A **66**, 013606 (2002)
20. K. Góral, L. Santos, M. Lewenstein, Phys. Rev. Lett. **88**, 170406 (2002)
21. B. Damski, L. Santos, E. Tiemann, M. Lewenstein, S. Kotochigova, P. Julienne, P. Zoller, Phys. Rev. Lett. **90**, 110401 (2003)
22. H.L. Bethlem, G. Berden, G. Meijer, Phys. Rev. Lett. **83**, 1558 (1999)
23. H.L. Bethlem, A.J.A. van Roij, R.T. Jongma, G. Meijer, Phys. Rev. Lett. **88**, 133003 (2002)
24. J.D. Weinstein, R. deCarvalho, T. Guillet, B. Friedrich, J.M. Doyle, Nature **395**, 148 (1998)
25. S.A. Rangwala, T. Junglen, T. Rieger, P.W.H. Pinkse, G. Rempe, Phys. Rev. A **64**, 043406 (2003)
26. B.S. Zhao, M. Castillejo, D.S. Chung, B. Friedrich, D. Herschbach, Rev. Sci. Instr. **75**, 146 (2004)
27. M. Mudrich et al., Eur. Phys. J. D **31**, 291 (2004)
28. A.J. Kerman, J.M. Sage, S. Sainis, T. Bergeman, D. DeMille, Phys. Rev. Lett. **92**, 033004 (2004)
29. U. Schlöder, C. Silber, T. Deuschle, C. Zimmermann, Phys. Rev. A **66**, 061403 (2002)
30. J.P. Shaffer, W. Chalupczak, N.P. Bigelow, Phys. Rev. Lett. **82**, 1124 (1999)
31. C. Haimberger, J. Kleinert, M. Bhattacharya, N.P. Bigelow, Phys. Rev. A **70**, 021402(R) (2004)
32. M.W. Mancini, G.D. Telles, A.R.L. Caires, V.S. Bagnato, L.G. Marcassa, Phys. Rev. Lett. **92**, 133203 (2004)
33. A.J. Kerman, J.M. Sage, S. Sainis, T. Bergeman, D. DeMille, Phys. Rev. Lett. **92**, 153001 (2004)
34. D. Wang et al., Eur. Phys. J. D **31**, 165 (2004)
35. H. Wang, W.C. Stwalley, J. Chem. Phys. **108**, 5767 (1998)
36. P. Pillet, A. Crubellier, A. Bleton, O. Dulieu, P. Nosbaum, I. Mourachko, F. Masnou-Seeuws, J. Phys. B **30**, 2801 (1997)
37. C.M. Dion, C. Drag, O. Dulieu, B. Laburthe Tolra, F. Masnou-Seeuws, P. Pillet, Phys. Rev. Lett. **86**, 2253 (2001)
38. C. Drag, B. Laburthe Tolra, O. Dulieu, D. Comparat, M. Vatasescu, S. Boussen, S. Guibal, A. Crubellier, P. Pillet, IEEE J. Quant. Electron. **36**, 1378 (2000)
39. P.S. Julienne, J. Res. Natl. Inst. Stand. Technol. **101**, 487 (1996)
40. J.L. Bohn, P.S. Julienne, Phys. Rev. A **60**, 414 (1999)
41. C. Amiot, O. Dulieu, J. Vergès, Phys. Rev. Lett. **83**, 2316 (1999)

42. V. Kokoouline, O. Dulieu, F. Masnou-Seeuws, Phys. Rev. A **62**, 022504 (2000)
43. M. Korek, A.R. Allouche, K. Fakhreddine, A. Chaalan, Can. J. Phys. **78**, 977 (2000)
44. A.R. Allouche, M. Korek, K. Fakherddine, A. Chaalan, M. Dagher, F. Taher, M. Aubert-Frécon, J. Phys. B **33**, 2307 (2000)
45. M. Korek, A.R. Allouche, M. Kobeissi, A. Chaalan, M. Dagher, K. Fakherddin, M. Aubert-Frécon, Chem. Phys. **256**, 1 (2000)
46. S. Rousseau, A.R. Allouché, M. Aubert-Frécon, J. Mol. Spectrosc. **203**, 235 (2000)
47. A. Derevianko, J.F. Babb, A. Dalgarno, Phys. Rev. A **63**, 052704 (2001)
48. K. Willner, O. Dulieu, F. Masnou-Seeuws, J. Chem. Phys. **120**, 548 (2004)
49. V. Kokoouline, O. Dulieu, R. Kosloff, F. Masnou-Seeuws, J. Chem. Phys. **110**, 9865 (1999)
50. N. Spies, Ph.D. thesis, Universität Kaiserslautern (1989)
51. D. Comparat, C. Drag, A. Fioretti, O. Dulieu, P. Pillet, J. Mol. Spectrosc. **195**, 229 (1999)
52. H. Skenderovic, R. Beuc, T. Ban, G. Pichler, Eur. Phys. J. D **19**, 49 (2002)
53. O. Docenko, M. Tamanis, R. Ferber, A. Pashov, H. Knöckel, E. Tiemann, Phys. Rev. A **69**, 042503 (2004)